

MAGICITY IN EXOTIC NUCLEI

G. Saxena^a, D. Singh^b, M. Kaushik^b

^a Department of Physics, Government Women Engineering College, Ajmer-305002, India

^b Department of Physics, University of Rajasthan, Jaipur-302006, India

Inspired by the recent experiments (Nature. 2012. V. 486. P. 341; Nature. 2009. V. 459. P. 1069), indicating doubly magic nuclei which lie near the drip-line and encouraged by the success of relativistic mean-field (RMF) plus state-dependent BCS approach for the description of the ground-state properties of the drip-line nuclei, we have further employed this approach, across the entire periodic table, to explore magic nuclei. In our RMF + BCS, approach, the single-particle continuum corresponding to the RMF is replaced by a set of discrete positive energy states for the calculations of pairing energy. Detailed analysis of the two-proton/neutron separation energy, single-particle spectrum, pairing energies and densities of the nuclei predicts that some of the traditional shell closures disappear in the vicinity of the drip-lines and some new shell closures emerge.

Основываясь на новых экспериментальных данных (Nature. 2012. V. 486. P. 341; Nature. 2009. V. 459. P. 1069) о дважды магических ядрах, которые лежат в области вблизи границы стабильности, и на успехах модели релятивистского среднего поля (RMF) совместно с зависящим от состояния приближением (BCS) в описании свойств основного состояния ядер на границе стабильности, в настоящей работе данное приближение используется для описания магических ядер всей периодической таблицы элементов. В приближении RMF + BCF одночастичный континуум, соответствующий RMF, заменяется набором дискретных состояний с положительной энергией и используется для вычисления энергии спаривания. Детальный анализ энергии разделения двух протонов/нейтронов, одночастичного спектра, энергий спаривания и плотностей ядер показывает, что некоторые традиционные замыкания оболочек исчезают в окрестности границы стабильности, но при этом появляются новые замыкания.

PACS: 21.10.-k; 21.60.Ev

INTRODUCTION

In 1949, Mayer, Haxel, Suess and Jensen [1, 2] independently showed that the observed shell closures at nucleon numbers 8, 20, 50, 82 and 126 could be explained by the inclusion of a spin-orbit potential. These special proton and/or neutron numbers were termed as «magic numbers». It referred to the fact that nuclei with these Z and/or N values had large gaps between occupied and empty single-particle states, and thus have strong stability against excitations to higher levels. A change in the spacing of single-particle levels in the region away from the valley of β stability gives rise to the shell gaps which are different from those observed for nuclei close to the valley of stability. Due to this reason, some

of the traditional magic numbers disappear in the exotic nuclei and new magic numbers emerge.

Experimental and theoretical studies of such exotic nuclei with extreme isospin values constitute one of the most active current areas of research in nuclear physics. Experiments [3–9] with radioactive nuclear beams provide the opportunity to study very short-lived nuclei with large $[N-Z]$ value. Further, in recent experiments with radioactive nuclear beams (RNB), disappearance of traditional magic numbers and appearance of new magic numbers have been observed in nuclei with exotic isospin ratios [8, 9]. More recently, it has been demonstrated in two independent experiments [5, 6] that ^{24}O , the heaviest isotope of oxygen with neutron number $N = 16$, is a doubly magic nucleus at neutron drip line. Towards proton drip line ^{100}Sn has also been found as a doubly magic nucleus by Hinke et al. [3] and towards neutron drip line reaction cross section of ^{22}C has been found significantly larger than those of its neighborhood isotopes, suggesting ^{22}C as a doubly magic halo nucleus [7].

Theoretical descriptions of drip-line nuclei in terms of a few-body model or clusters [10, 11], shell-model [12, 13] and mean-field theories, both nonrelativistic [14, 15] as well as relativistic mean field (RMF) [16–30] have been well obtained. The advantage of the RMF approach is that it provides the spin-orbit interaction in the entire mass region, which is consistent with the nuclear density [20]. This indeed has been found to be very important for the study of unstable nuclei near the drip-line [19]. It has been shown [27, 28] that the relativistic mean-field (RMF) plus BCS approach wherein the continuum has been replaced by the discrete single-particle states for the calculation of the pairing energy provides an alternative fast approach to the relativistic Hartree–Fock–Bogoliubov (RHB) description [22, 26] of the drip-line nuclei.

Encouraged by the success of our RMF + BCS approach [27, 28], and the impetus provided by the recent experimental developments, especially the measurements [3–7], we have employed it for the study of structure of even–even nuclei covering the whole periodic region up to the drip-lines ($8 \leq Z \leq 82$ and $8 \leq N \leq 126$) to investigate the unusual proton and neutron magic numbers and doubly magic nucleus. The shell closures with pronounced gaps between shells in nuclei endow them with spherical shape. Consequently, the magic nuclei are characterized by zero deformation. In our systematic investigations we first carry out RMF + BCS calculations including the deformation degree of freedom [30] (to be referred to throughout as deformed RMF + BCS) to identify magic numbers from two-neutron/proton separation energy and to establish whether the entire chain of magic isotones/isotopes for a given neutron/proton number is indeed spherical or not.

In the case of negligible/zero deformation, we take advantage of the RMF + BCS approach for spherical shapes [27] (to be referred to throughout as spherical RMF + BCS) for the analysis of results in terms of spherical single-particle wave functions and energy levels to make the discussion of shell closures and magicity, etc., more convenient and transparent. Also, behavior of the single-particle states near the Fermi surface which in turn plays an important role near the drip-line can be easily understood. Moreover, within such a framework, contributions of neutron and proton single-particle states to the density profiles, pairing gaps, total pairing energy, etc., which are also equally important in the study of exotic phenomena, can be demonstrated with clarity. This approach indeed turns out to be very useful for the study of poorly understood exotic nuclei.

1. RELATIVISTIC MEAN-FIELD THEORY

Our RMF calculations have been carried out using the model Lagrangian density with nonlinear terms for both the σ and ω mesons along with the TMA parametrization as described in detail in [19, 27]:

$$\begin{aligned} \mathcal{L} = & \bar{\psi}[\gamma^\mu \partial_\mu - M]\psi + \frac{1}{2} \partial_\mu \sigma \partial^\mu \sigma - \frac{1}{2} m_\sigma^2 \sigma^2 - \frac{1}{3} g_2 \sigma^3 - \frac{1}{4} g_3 \sigma^4 - g_\sigma \bar{\psi} \sigma \psi - \\ & - \frac{1}{4} H_{\mu\nu} H^{\mu\nu} + \frac{1}{2} m_\omega^2 \omega_\mu \omega^\mu + \frac{1}{4} c_3 (\omega_\mu \omega^\mu)^2 - g_\omega \bar{\psi} \gamma^\mu \psi \omega_\mu - \\ & - \frac{1}{4} G_{\mu\nu}^a G^{a\mu\nu} + \frac{1}{2} m_\rho^2 \rho_\mu^a \rho^{a\mu} - g_\rho \bar{\psi} \gamma_\mu \tau^a \psi \rho^{\mu a} - \frac{1}{4} F_{\mu\nu} F^{\mu\nu} - e \bar{\psi} \gamma_\mu \frac{(1 - \tau_3)}{2} A^\mu \psi, \end{aligned} \quad (1)$$

where the field tensors H , G and F for the vector fields are defined by

$$\begin{aligned} H_{\mu\nu} &= \partial_\mu \omega_\nu - \partial_\nu \omega_\mu, \\ G_{\mu\nu}^a &= \partial_\mu \rho_\nu^a - \partial_\nu \rho_\mu^a - 2g_\rho \epsilon^{abc} \rho_\mu^b \rho_\nu^c, \\ F_{\mu\nu} &= \partial_\mu A_\nu - \partial_\nu A_\mu, \end{aligned}$$

and other symbols have their usual meaning. Based on the single-particle spectrum calculated by the RMF described above, we perform state-dependent BCS calculations [31, 32]. As we already mentioned, the continuum is replaced by a set of positive-energy states generated by enclosing the nucleus in a spherical box. Thus, the gap equations have the standard form for all the single-particle states, i.e.,

$$\Delta_{j_1} = -\frac{1}{2} \frac{1}{\sqrt{2j_1 + 1}} \sum_{j_2} \frac{\langle (j_1^2) 0^+ | V | (j_2^2) 0^+ \rangle}{\sqrt{(\varepsilon_{j_2} - \lambda)^2 + \Delta_{j_2}^2}} \sqrt{2j_2 + 1} \Delta_{j_2}, \quad (2)$$

where ε_{j_2} are the single-particle energies, and λ is the Fermi energy, whereas the particle number condition is given by $\sum_j (2j + 1) v_j^2 = N$. In the calculations we use for the pairing interaction a delta force, i.e., $V = -V_0 \delta(r)$ with the same strength V_0 for both protons and neutrons. The value of the interaction strength $V_0 = 350 \text{ MeV} \cdot \text{fm}^3$ was determined in [27] by obtaining a best fit to the binding energy of Ni isotopes. We use the same value of V_0 for our present studies of isotopes of other nuclei as well. Apart from its simplicity, the applicability and justification of using such a δ -function form of interaction has recently been discussed in [14], whereby it has been shown in the context of HFB calculations that the use of a delta force in a finite-space simulates the effect of finite-range interaction in a phenomenological manner (see also [33] and [34] for more details). The pairing matrix element for the δ -function force is given by

$$\langle (j_1^2) 0^+ | V | (j_2^2) 0^+ \rangle = -\frac{V_0}{8\pi} \sqrt{(2j_1 + 1)(2j_2 + 1)} I_R, \quad (3)$$

where I_R is the radial integral having the form

$$I_R = \int dr \frac{1}{r^2} (G_{j_1}^* G_{j_2} + F_{j_1}^* F_{j_2})^2. \quad (4)$$

Here G_α and F_α denote the radial wave functions for the upper and lower components, respectively, of the nucleon wave function expressed as

$$\psi_\alpha = \frac{1}{r} \begin{pmatrix} i G_\alpha \mathcal{Y}_{j_\alpha l_\alpha m_\alpha} \\ F_\alpha \sigma \cdot \hat{r} \mathcal{Y}_{j_\alpha l_\alpha m_\alpha} \end{pmatrix}, \quad (5)$$

and satisfy the normalization condition

$$\int dr \{|G_\alpha|^2 + |F_\alpha|^2\} = 1. \quad (6)$$

In Eq.(5), the symbol \mathcal{Y}_{jlm} has been used for the standard spinor spherical harmonics with the phase i^l . The coupled field equations obtained from the Lagrangian density in (1) are finally reduced to a set of simple radial equations [18] which are solved self-consistently along with the equations for the state-dependent pairing gap Δ_j and the total particle number N for a given nucleus.

The relativistic mean-field description has been extended for the deformed nuclei of axially symmetric shapes by Gambhir, Ring and their collaborators [35] using an expansion method. The treatment of pairing has been carried out in [30] using state-dependent BCS method [31] as has been given by Yadav et al. [27] for the spherical case. For axially deformed nuclei, the rotational symmetry is no more valid and the total angular momentum j is no longer a good quantum number. Nevertheless, the various densities still are invariant with respect to a rotation around the symmetry axis. Here we have taken the symmetry axis to be the z axis. Following Gambhir et al. [35], it is then convenient to employ the cylindrical coordinates.

The scalar, vector, isovector and charge densities, as in the spherical case, are expressed in terms of the spinor π_i , its conjugate π_i^+ , operator τ_3 , etc. These densities serve as sources for the fields $\phi = \sigma, \omega^0, \rho^0$ and A^0 , which are determined by the Klein–Gordon equation in cylindrical coordinates. Thus, a set of coupled equations, namely, the Dirac equation with potential terms for the nucleons and the Klein–Gordon-type equations with sources for the mesons and the photon, is obtained. These equations are solved self-consistently. For this purpose, as described above, the well-tested basis expansion method has been employed [35]. The bases used here are generated by an anisotropic (axially symmetric) harmonic oscillator potential. The upper and lower components of the nucleon spinors, the fields as well as the baryon currents and densities, are expanded separately in these bases. The expansion is truncated so as to include all the configurations up to a certain finite value of the major oscillator shell quantum number. In this expansion method, the solution of the Dirac equation gets reduced to a symmetric matrix diagonalization problem, while that of the Klein–Gordon equation reduces to a set of inhomogeneous equations. The solution provides the spinor fields, and the nucleon currents and densities (sources of the fields), from which all the relevant ground-state nuclear properties are calculated. For further details of these formulations, we refer the reader to [30,35].

2. RESULTS AND DISCUSSIONS

2.1. Neutron Shell Closures. In order to investigate the effect of isospin on traditional neutron shell closures, we plot in Fig.1 the two-neutron separation energy S_{2n} obtained in deformed RMF approach for the even–even nuclei with different isospin values $T_Z = (N - Z)/2$ ranging from -3 to 15 as a function of neutron number N . In this figure,

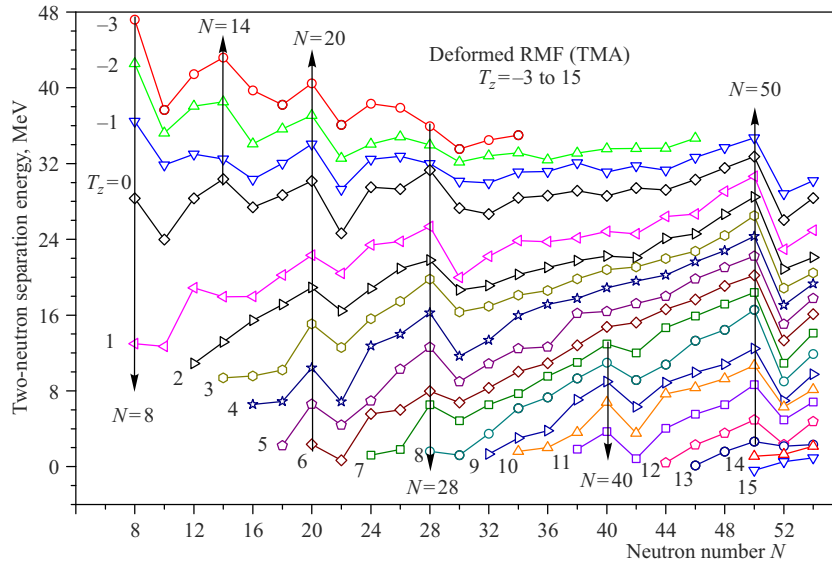


Fig. 1. The two-neutron separation energy S_{2n} obtained within the deformed RMF approach. The lines connect the nuclei with the same isospin value $T_Z = (N - Z)/2 = -3$ to 15. At the magic numbers a sudden decrease in the separation energy is evidently seen

the results for nuclei with neutron number N only up to 54 have been displayed. Plot of S_{2n} covering nuclei with higher N exhibiting similar characteristics has not been displayed here in order to keep the figure uncluttered. In Fig. 1, and in similar plots for heavier nuclei, a sudden decrease in the two-neutron separation energies S_{2n} is clearly seen at the major shell closures corresponding to traditional neutron magic numbers $N = 8, 20, 28, 50, 82$ and 126 . These major neutron shells are seen generally to persist well into the regions belonging to the proton-rich as well as neutron-rich nuclei while approaching the drip-lines. For these magic numbers the chains of bound isotones are relatively large. Such magic numbers may be termed as strong magic numbers. However, there are instances, especially for neutron-rich cases, whereby a major shell structure is weakened and the associated magic number disappears with the emergence of a new magic number.

It is seen in Fig. 1 that the traditional neutron shell closure at $N = 50$ disappears for the nucleus ^{70}Ca ($T_Z = 15$) lying in the vicinity of two-neutron drip-line of the Ca isotopic chain. It may be mentioned that the deformed RMF calculations show that the nucleus ^{70}Ca is just unbound with very small negative two-neutron separation energy (~ -400 keV). However, we have taken the nucleus ^{70}Ca for the present description as a bound one despite a very small negative value of the two-neutron separation energy implying an unbound nucleus. Similarly, it is found that the neutron shell closure at $N = 28$ disappears for the nucleus ^{40}Mg ($T_Z = 8$) lying at the two-neutron drip-line of the nuclei corresponding to the $N = 28$ isotonic chain. Another important result that can be seen from Fig. 1 is the emergence of new shell closures at the neutron number $N = 40$ (for $T_Z = 7$ to 11) and $N = 14$ (for $T_Z = -3$ to 0). Consequently, a shell closure at $N = 40$ is found for the nuclei ^{58}Ar , ^{60}Ca , ^{62}Ti , ^{64}Cr and ^{66}Fe . Similarly, the calculated results show that the neutron shell closure occurs at $N = 14$ for the nuclei ^{28}Si , ^{30}S , ^{32}Ar and ^{34}Ca .

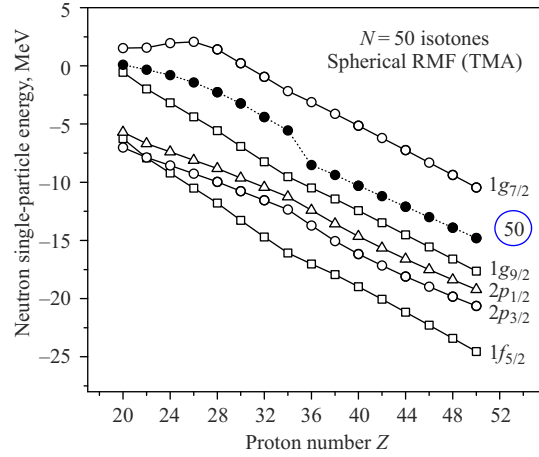


Fig. 2. Variation of the neutron single-particle energies obtained within the spherical RMF calculations for the $N = 50$ isotonic chain with increasing proton number Z . The neutron Fermi level has been shown by filled circles connected by solid line

In order to gain some more evidence for the disappearance of traditional shell closures at the neutron number $N = 28$ and $N = 50$, and likewise the appearance of new shell closures at $N = 14$ and $N = 40$, we present here a detailed study of the calculated results for the radial density distribution and the single-particle spectra of the spherical nuclei identified from the deformed RMF calculations. The results of the deformed RMF calculations for the $N = 50$ isotonic chain show that all the nuclei with neutron number $N = 50$ are spherical in shape with zero deformation. Therefore, in order to understand the disappearance of the neutron shell closure at $N = 50$ in the vicinity of the neutron drip-line, we employ spherical RMF approach to obtain the neutron single-particle spectrum of the nuclei belonging to $N = 50$ isotonic chain. These results have been displayed in Fig.2 as a function of increasing proton number Z .

It is readily seen in Fig.2 that the large energy gap between the single-particle levels $1g_{9/2}$ and $1g_{7/2}$ which is responsible for the traditional neutron shell closure at $N = 50$ is significantly reduced due to the changed characteristics of the spin-orbit splitting for the neutron-rich drip-line nucleus ^{70}Ca having a large isospin value ($T_Z = 15$). Due to this behavior of neutron single-particle states, shell closure at the traditional neutron magic number $N = 50$ is found to disappear. This result is also supported by the nonzero neutron pairing energy value (-2.99 MeV) for the neutron-rich nucleus ^{70}Ca ($T_Z = 15$). Further, from the deformed RMF calculations it is found that nuclei with $Z = 18-40$ belonging to $N = 40$ isotonic chain have the spherical shape, whereas all the nuclei (except ^{22}O and ^{34}Ca) which belong to the $N = 14$ isotonic chain are deformed. With this in view, we have employed the spherical RMF approach only for the $N = 40$ isotonic chain to obtain the neutron single-particle spectrum.

The results obtained from the spherical RMF calculations have been displayed in Fig. 3. It is evident that the large energy gap between the neutron single-particle levels $2p_{1/2}$ and $1g_{9/2}$ is responsible for the shell closure which is found to occur for the neutron number $N = 40$ in the nuclei with proton number $Z = 18$ to 26. However, this gap starts to diminish for the

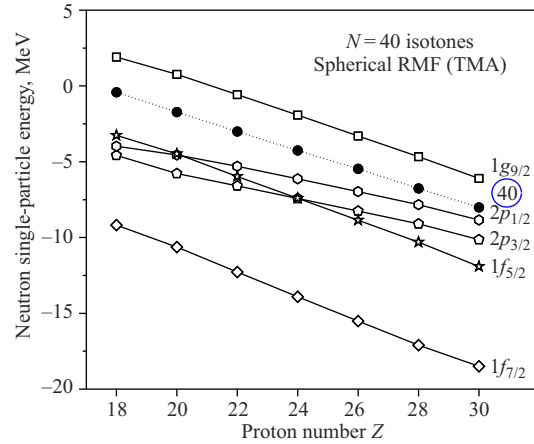


Fig. 3. Variation of the neutron single-particle energies obtained within the spherical RMF calculations for the $N = 40$ isotonic chain with increasing proton number Z . The neutron Fermi level has been shown by filled circles connected by solid line

nuclei with $Z > 26$ resulting in the disappearance of the magic number $N = 40$. Again these results are also supported by the nonzero neutron pairing energy value for the neutron-rich nuclei ^{68}Ni ($T_Z = 6$) and ^{70}Zn ($T_Z = 5$).

In Fig. 4, we have displayed the results of spherical RMF approach for the neutron single-particle spectrum for the $Z = 20$ isotopic chain. It is clearly seen from the figure that the large energy gaps between single-particle levels $1d_{5/2}$ and $1d_{3/2}$, and that between the levels $2p_{1/2}$ and $1g_{9/2}$ are responsible for the neutron shell closures in the Ca isotopes for the neutron number $N = 14$ and $N = 40$ apart from the traditional shell closures at $N = 20$ and $N = 28$. As mentioned earlier, the $N = 50$ shell closure is seen to disappear due to the absence of the gaps between the single-particle states $1g_{9/2}$ and $1g_{7/2}$ near drip line.

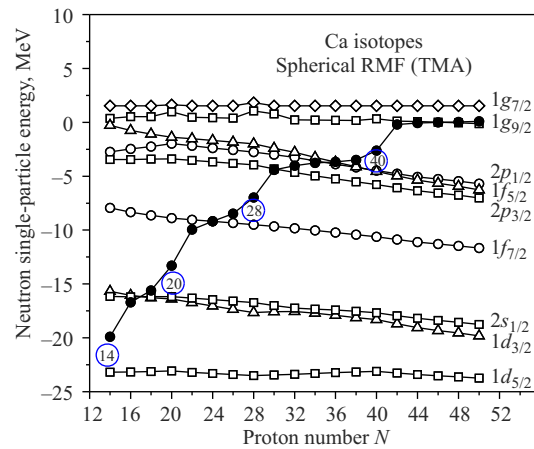


Fig. 4. Variation of the neutron single-particle energies obtained within the spherical RMF approach for the Ca ($Z = 20$) isotopes with increasing neutron number N . The neutron Fermi level has been shown by filled circles connected by solid line

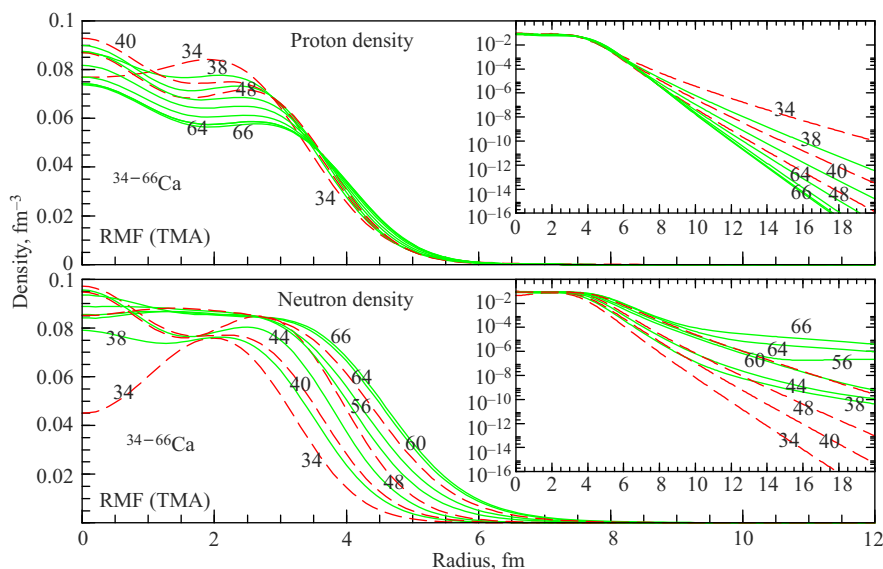


Fig. 5. The upper and lower panels, respectively, show the proton and neutron density distributions for the Ca isotopes. The numbers on the density distribution lines indicate the mass number of the Ca isotope. The insets show the results on a logarithmic scale up to rather large distances

These conclusions are further supported by the results of the calculated densities for the $Z = 20$ isotopic chain displayed in the lower panel of Fig. 5. Evidently, for the neutron number $N = 14, 20, 28$ and 40 , the neutron densities fall off rapidly and have smaller tails as compared to the isotopes with other neutron numbers. This sharp fall in asymptotic density values is due to the fact that for the closed shell isotopes there are no contribution to the density from the quasi-bound states having positive energy even though they are located close to zero energy near the continuum threshold.

2.2. Proton Shell Closures. Analogously to our investigations described in the preceding section, we have carried out the study of the behavior of traditional proton shell closures to identify the disappearance of traditional magic numbers or the emergence of the new magic numbers as we approach the drip-lines. To illustrate this, we have plotted in Fig. 6 the two-proton separation energy S_{2p} obtained in the deformed RMF approach for the even-even nuclei with different isospin values $T_Z = (N - Z)/2$ ranging from -3 to 15 as a function of proton number Z . As seen from Fig. 6 and from the similar plot for the higher Z values (not shown here), a sudden decrease is observed in the two-proton separation energy S_{2p} at the traditional proton magic numbers $Z = 8, 20, 28, 50$ and 82 . Similarly to the emergence of new neutron shell closure at $N = 14$, a new proton shell closure at $Z = 14$ is seen for the nuclei $^{26-42}\text{Si}$ ($T_Z = -1$ to 7).

Moreover, similar to the case of neutron shell closure at $N = 50$ which is found to be absent in the neutron-rich nuclei located in the vicinity of neutron drip-line, the proton shell closure at $Z = 50$ is found to disappear near the proton drip-line for the nuclei with high isospin values, for example, in the nucleus ^{176}Sn .

In order to get an insight into the proton magic number $Z = 14$, we have carried out a detailed study of proton single-particle energy variations obtained by employing spheri-

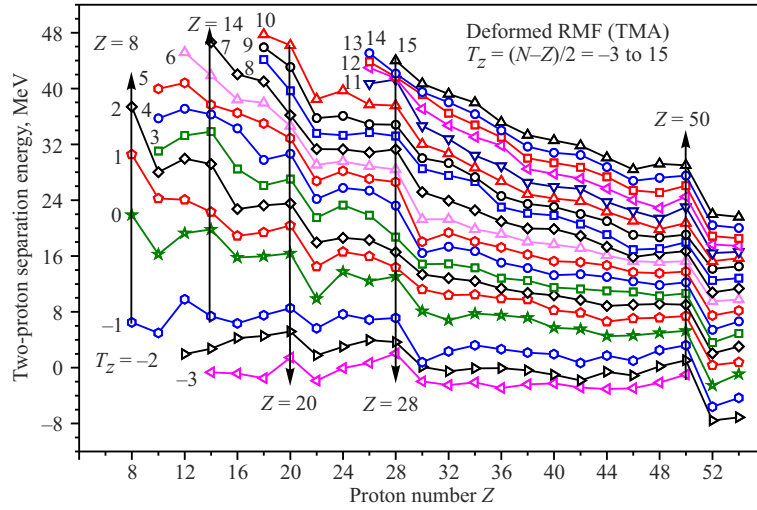


Fig. 6. Calculated results obtained within the deformed RMF approach showing the variation of two-proton separation energy S_{2p} with increasing proton number Z . The lines connect the nuclei with the same isospin value $T_Z = (N - Z)/2 = -3$ to 15 . At the magic numbers a sudden decrease in the separation energy is evidently seen

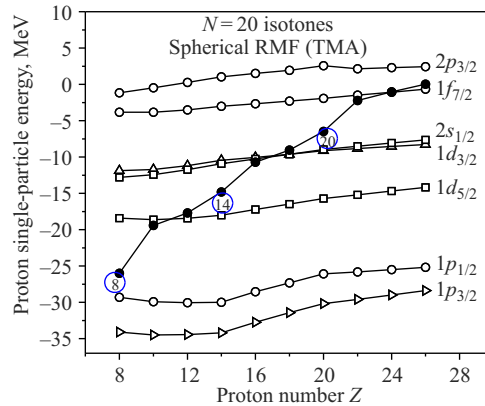


Fig. 7. Variation of the proton single-particle energies obtained within the spherical RMF approach for the $N = 20$ isotones with increasing proton number Z . The proton Fermi level has been shown by filled circles connected by solid line

cal RMF approach for the isotonic chain of spherical nuclei corresponding to the neutron number $N = 20$. For the purpose of illustration, we have shown in Fig. 7 such a variation of the proton single-particle energies obtained, in the spherical RMF calculation for the $N = 20$ isotonic chain.

The bound isotones for this chain have proton number ranging from $Z = 8$ to $Z = 26$. An appreciable gap between the proton single-particle states $1d_{5/2}$ and $1d_{3/2}$ are responsible for the occurrence of proton shell closure for the proton number $Z = 14$. Traditional proton shell closures at $Z = 8$ and 20 are seen to exist due to large energy gaps between occupied

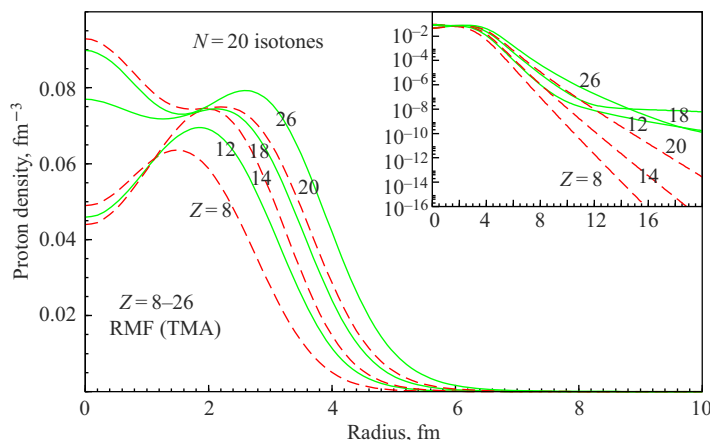


Fig. 8. The variation in the radial dependence of the proton density with increasing proton number Z for the nuclei belonging to the isotonic chain with neutron number $N = 20$. These results have been obtained within the spherical RMF approach. The numbers on the lines representing density profile indicate the proton number Z . The inset shows the results on a logarithmic scale up to rather large radial distances. Long dashes depict isotones which exhibit proton shell closure

and empty proton single-particle states. Another important conclusion which is drawn from Fig. 6 is that in contrast to the case of neutron shell closure at $N = 40$, no proton shell closure is seen at proton number $Z = 40$.

These conclusions are further supported by the results of the calculated densities for the $N = 20$ isotonic chain displayed in Fig. 8. The proton densities of the $N = 20$ isotones reveal that for the proton numbers $Z = 8, 14$ and 20 which correspond to proton shell closure in the nuclei ^{28}O , ^{34}Si and ^{40}Ca , respectively, the density distribution is rather confined to smaller radial distances and diminishes quickly, as is indicated by the slope of these curves. The densities for the isotones with sharp falloff have been represented by long dashed lines, and for the purpose of clarity this falloff has been shown as an inset for large distances in a logarithmic plot, as can be seen in Fig. 8.

3. SUMMARY

Inspired by the recent experiments [3–7] indicating doubly magic nuclei and encouraged by the success of our relativistic mean-field (RMF) plus state-dependent BCS approach for the description of the ground-state properties of the drip-line nuclei [27,28], we have further employed this approach, across the entire periodic table, to explore the unusual shell closures and doubly magic nuclei.

The Lagrangian density with nonlinear terms for the σ and ω mesons along with the TMA force parameters [19] has been employed for the purpose. State-dependent BCS calculations employing a delta-function interaction with the same interaction strength throughout have been performed for the pairing correlation energy. The calculated results comprising the systematics for the two-neutron and two-proton separation energies, single-particle energy and the neutron and proton density distribution profiles have been analyzed to predict the

possible magic numbers, and to explore and examine the disappearance of traditional magic numbers. It is found from the results for the even–even nuclei covering the range $8 \leq Z \leq 82$ that the appearance and disappearance of magic numbers near the drip-lines is quite a prevalent characteristic found amongst the drip-line nuclei. We have also presented the results of two-proton separation energy with increasing proton number and two-neutron separation energy with increasing neutron number for different isospin values. This is found very helpful to check the dependence of traditional shell closures on the isospin.

It has been demonstrated that the traditional neutron shell closure at $N = 50$ disappears for the nucleus ^{70}Ca ($T_Z = 15$) lying in the vicinity of two-neutron drip-line of the Ca isotopic chain. Similarly, neutron shell closure at $N = 28$ disappears for the nucleus ^{40}Mg ($T_Z = 8$) lying at the two-neutron drip-line of $N = 28$ isotonic chain. Another important result is emergence of new shell closures at $N = 40$ (for $T_Z = 7$ to 11) and $N = 14$ (for $T_Z = -3$ to 0). Consequently, $N = 40$ is found to be a shell closure for the nuclei ^{58}Ar , ^{60}Ca , ^{62}Ti , ^{64}Cr and ^{66}Fe , whereas $N = 14$ corresponds to shell closure for the nuclei ^{28}Si , ^{30}S , ^{32}Ar and ^{34}Ca . Similarly to the case of new neutron shell closure at $N = 14$, a new proton shell closure at $Z = 14$ is seen for the nuclei $^{26-42}\text{Si}$ ($T_Z = -1$ to 7). Moreover, similarly to the case of neutron shell closure at $N = 50$, which has been found to be absent in the neutron-rich nuclei located in the vicinity of neutron drip-line, the proton shell closure $Z = 50$ is found to disappear near the proton drip-line for the nuclei with extreme high isospin value, for example, in nucleus ^{176}Sn . These results are found to be consistent with the experimental systematics [36] of two-proton and two-neutron separation energies, S_{2p} and S_{2n} , respectively.

Acknowledgements. The authors are grateful to Prof. H.L. Yadav for his kind hospitality and guidance while visiting Banaras Hindu University, Varanasi, India. The authors are indebted to Dr. L. S. Geng, RCNP, Osaka, Japan, for valuable correspondence. The authors are also grateful to Prof. Hiroshi Toki, RCNP, Osaka University, Japan, for his valuable and encouraging suggestions.

REFERENCES

1. *Goepfert-Mayer M.* // Phys. Rev. 1949. V. 75. P. 1969.
2. *Haxel O., Jensen J. H. D., Suess H. E.* // Ibid. P. 1766.
3. *Hinke C. B. et al.* // Nature. 2012. V. 486. P. 341.
4. *Janssens Robert V. F.* // Nature. 2009. V. 459. P. 1069.
5. *Kanungo R. et al.* // Phys. Rev. Lett. 2009. V. 102. P. 152501.
6. *Hoffman C. R. et al.* // Phys. Lett. B. 2009. V. 672. P. 17.
7. *Tanaka K. et al.* // Phys. Rev. Lett. 2010. V. 104. P. 62701.
8. *Tanihata I.* // J. Phys. G. 1996. V. 22. P. 157;
Tanihata I. et al. // Phys. Lett. B. 2001. V. 512. P. 261.
9. *Ozawa A. et al.* // Phys. Rev. Lett. 2000. V. 84. P. 5493;
Ozawa A. et al. // Nucl. Phys. A. 2002. V. 709. P. 60.
10. *Jensen A. et al.* // Rev. Mod. Phys. 2004. V. 76. P. 215;
Jensen A. S., Riisager K. // Phys. Lett. B. 2000. V. 480. P. 39.
11. *Dasgupta S., Mazumdar I., Bhasin V. S.* // Phys. Rev. C. 1994. V. 50. P. 551(R).

12. *Bertsch G., Esbensen H., Sushch A.* // Phys. Rev. C. 1990. V. 42. P. 758;
Bertsch G., Foxwell J. // Ibid. V. 41. P. 1300.
13. *Otsuka T. et al.* // Phys. Rev. Lett. 2001. V. 87. P. 082502.
14. *Dobaczewski J. et al.* // Phys. Rev. C. 1996. V. 53. P. 2809;
Bennaceur K., Dobaczewski J., Ploszajczak M. // Phys. Lett. B. 2000. V. 496. P. 154.
15. *Grasso M. et al.* // Phys. Rev. C. 2001. V. 64. P. 064321.
16. *Serot B. D., Walecka J. D.* // Adv. Nucl. Phys. 1986. V. 16. P. 1.
17. *Reinhard P. G.* // Rep. Prog. Phys. 1989. V. 52. P. 439.
18. *Reinhard P. G. et al.* // Z. Phys. A. 1986. V. 323. P. 13.
Mizutori S. et al. // Phys. Rev. C. 2000. V. 61. P. 044326.
19. *Sugahara Y., Toki H.* // Nucl. Phys. A. 1994. V. 579. P. 557.
Sugahara Y. Ph. D. Thesis. Tokyo Metropolitan Univ., 1995.
20. *Brockman R., Toki H.* // Phys. Rev. Lett. 1992. V. 68. P. 3408.
21. *Ring P.* // Nucl. Part. Phys. 1998. V. 24. P. 1467;
Vretenar D. et al. // Phys. Rev. Lett. 2003. V. 91. P. 262502.
22. *Lalazissis G. A., Vretenar D., Ring P.* // Phys. Rev. C. 1998. V. 57. P. 2294.
23. *Sharma M. M., Nagarajan M. A., Ring P.* // Phys. Lett. B. 1993. V. 312. P. 377.
24. *Estal M. Del et al.* // Phys. Rev. C. 2001. V. 63. P. 044321.
25. *Meng J.* // Phys. Rev. C. 1998. V. 57. P. 1229; Nucl. Phys. A. 1998. V. 635. P. 3.
26. *Meng J. et al.* // Phys. Rev. C. 2002. V. 65. P. 041302(R);
Meng J. et al. // Prog. Part. Nucl. Phys. C. 2006. V. 57. P. 470.
27. *Yadav H. L., Kaushik M., Toki H.* // Intern. J. Mod. Phys. E. 2004. V. 13. P. 647;
Kaushik M., Singh D., Yadav H. L. // Acta Phys. Slov. 2005. V. 5.(2). P. 181.
28. *Yadav H. L., Sugimoto S., Toki H.* // Mod. Phys. Lett. A. 2002. V. 17. P. 2523;
Saxena G. et al. // Mod. Phys. Lett. A. 2008. V. 23. P. 2589;
Singh D., Saxena G. // Intern. J. Mod. Phys. E. 2012. V. 21, No. 9. P. 1250076.
29. *Todd-Rutel B. G., Piekarewicz J., Cottle P. D.* // Phys. Rev. C. 2004. V. 69. P. 021301.
30. *Geng L. S.* Ph. D. Thesis. RCNP, Osaka University. Osaka, 2005;
Geng L. S. et al. // Prog. Theor. Phys. 2003. V. 110. P. 921.
31. *Lane A. M.* Nuclear Theory. Benjamin, 1964.
32. *Ring P., Schuck P.* The Nuclear Many-Body Problem. Springer, 1980.
33. *Bertsch G. F., Esbensen H.* // Ann. Phys. (N.Y.). 1991. V. 209. P. 327.
34. *Migdal A. B.* Theory of Finite Fermi Systems and Applications to Atomic Nuclei. N. Y.: Intersci., 1967.
35. *Gambhir Y. K., Ring P., Thimet A.* // Ann. Phys. (N. Y.). 1990. V. 198. P. 132;
Ring P., Gambhir Y. K., Lalazissis G. A. // Comp. Phys. Commun. 1997. V. 105. P. 77.
36. *Audi G., Wapstra A. H., Thibault C.* // Nucl. Phys. A. 2003. V. 729. P. 337.

Received on August 20, 2012.